# Inconel 718-W7Ni3Fe bimetallic structures using directed energy depositionbased additive manufacturing

C. Groden<sup>1</sup>, Kellen D. Traxel<sup>1</sup>, Ali Afrouzian<sup>1</sup>, E. Nyberg<sup>2</sup>, A. Bandyopadhyay<sup>1</sup>

<sup>1</sup> W. M. Keck Biomedical Materials Research Laboratory

School of Mechanical and Materials Engineering

Washington State University, Pullman, WA 99164, USA

<sup>2</sup> Tungsten Parts Wyoming, Laramie, WY 82070

E-mail: amitband@wsu.edu

#### Abstract

Bimetallic structures produced via additive manufacturing (AM) have demonstrated outstanding potential for improving the properties of high-temperature structures. To this end, it was hypothesized in this study that using a tungsten alloy would increase the thermal conductivity of the bimetallic structure compared to pure Inconel 718. Bimetallic structures of Inconel 718 and W7Ni3Fe were manufactured using directed energy deposition (DED)-based AM. Hardness, thermal analysis by diffusivity measurement, and compression testing were done to evaluate the effect of tungsten alloy deposition on Inconel 718's thermal and mechanical properties. Bimetallic structures of Inconel 718-W alloy containing a 50-50 volume % of each displayed a 100% improvement in thermal diffusivity compared to pure Inconel 718, with extensive mixing and remelting due to laser processing. Furthermore, the bimetallic compression samples showed a 100% increase in yield strength combined with a 50% reduction in modulus of elasticity compared to Inconel 718.

*Keywords*: Inconel 718; Additive manufacturing; Tungsten alloy; Bimetallic structures; Additive manufacturing.

#### 1.0 Introduction

Advances in directed energy deposition (DED) based additive manufacturing has allowed for the manufacturing of novel composites with unique micro- and macrostructures, improving the properties and performance of lesser capable materials in specific applications. Tailored design of composite structures enables something different mechanically or thermally from its constituents, resulting in a part where the properties are better than the constituents alone. Furthermore, these composite materials have exhibited reduced flammability, improved wear and corrosion resistance, and increased cost-efficiency when comparing the ratio of price to performance [1]. Some examples include premixed composites of CaP reinforced CoCrMo for the articulating surfaces of load-bearing implants to improve the wear resistance and reduce toxic metal ion release such as Co<sup>2+</sup> [2]. Similarly, increasing the fine Al13Fe4 to coarse Al13Fe4 laths in aluminum matrix composites increases the hardness and strength [3]. Another class of composites is functionally graded materials (FGMs), where the composition gradually changes within a material to provide site-specific enhancement of one or more properties in a particular direction. This allows for materials with particular properties to be created without the need for complex joining between difficult to weld materials [4]. Some examples of AM processed FGMs include Ti6Al4V and Invar composites [5] and Inconel 625 and 304L stainless steel [6]. A material system that could benefit from this type of structure is nickel-based superalloys, such as Inconel 718, which exhibit outstanding high-temperature stability and properties but suffer from low thermal conductivity. However, this property can significantly limit designs and applications because of the inability to effectively distribute heat away from critical components at high temperatures, motivating manufacturing approaches towards influencing thermal conductivity while maintaining the high-temperature properties of the base material.

One approach that has seen success addressing thermal conductivity is bimetallic structures, where one metal is deposited directly onto another, creating a region of site-specific properties. One of the main processing advantages of bimetallic materials is that composition is not limited. Furthermore, there will likely be an interfacial reaction in these bimetallic structures, forming a robust interface and strengthening the entire material. However, this can cause a weak or brittle interface in some material systems. Bimetallic interfaces can also exhibit other unique properties such as thermal stability [7]. Some of the AM processed bimetallic structures include

Inconel 625 to copper [8], 316L stainless steel to CuSn10 [9], Inconel 718 to Ti6Al4V [10], and maraging steel to H13 steel [11]. NASA reported using Inconel/GRCop84 alloy bimetallic structures in heat exchangers and channel-cooled nozzles [12]. These studies have reported enhanced mechanical properties, thermal conductivity, or oxidation resistance. If the two materials do not bond well to one another, an interlayer can be used to improve the adhesion of both materials [13,14]. Due to the better practicality and likelihood of a strong interface, nickel-based superalloys would best benefit from forming this type of composite.

Tungsten alloys are known for their high thermal conductivity, hardness, strength, and performance at high temperatures [15], making them a viable candidate for improving the properties of lesser-performing materials. Tungsten-based alloys and composites are the solid materials of choice for plasma-facing components (PFCs) of future fusion reactors, such as the International Thermonuclear Experimental Reactor (ITER), and have been the subject of research in this area [16]. Tungsten alloys are also commonly used in aerospace and ballistic applications [17,18]. These alloys consist of about 90% tungsten combined with ductile, lower melting metals such as nickel and iron [15]. The ductile metal content allows the alloy to be liquid-phase sintered or cast at lower temperatures while the tungsten stays solid throughout manufacturing. Only a few methods, such as plasma arc welding, can melt tungsten, as it has a very high melting point, >3400 °C. The density of tungsten is also high (~16g/cc), making it unusable in cases where performance to weight efficiency is critical to the success of the part. The weldability of Inconel 718 is explicitly high, making it one of the most used alloys in metal additive manufacturing [19]. The density of Inconel 718 is nearly half that of tungsten alloys, ~8 g/cc. Therefore, it makes sense that a bimetallic of the two alloys would improve the thermal and mechanical properties compared to pure Inconel 718. Other works had seen success in a similar approach, where a 250% increase in thermal diffusivity is reported when GRCop-84 was added to Inconel 718 [20]. In this work, bimetallic structures of Inconel 718 and W7Ni3Fe have been processed using the directed energy deposition (DED)-based AM. An overview of the bimetallic application and DED additive manufacturing is shown in Figure 1. These bimetallic structures have been characterized using the SEM and EDS for microstructural analysis, thermal diffusivity, uniaxial compression for mechanical properties, and hardness.

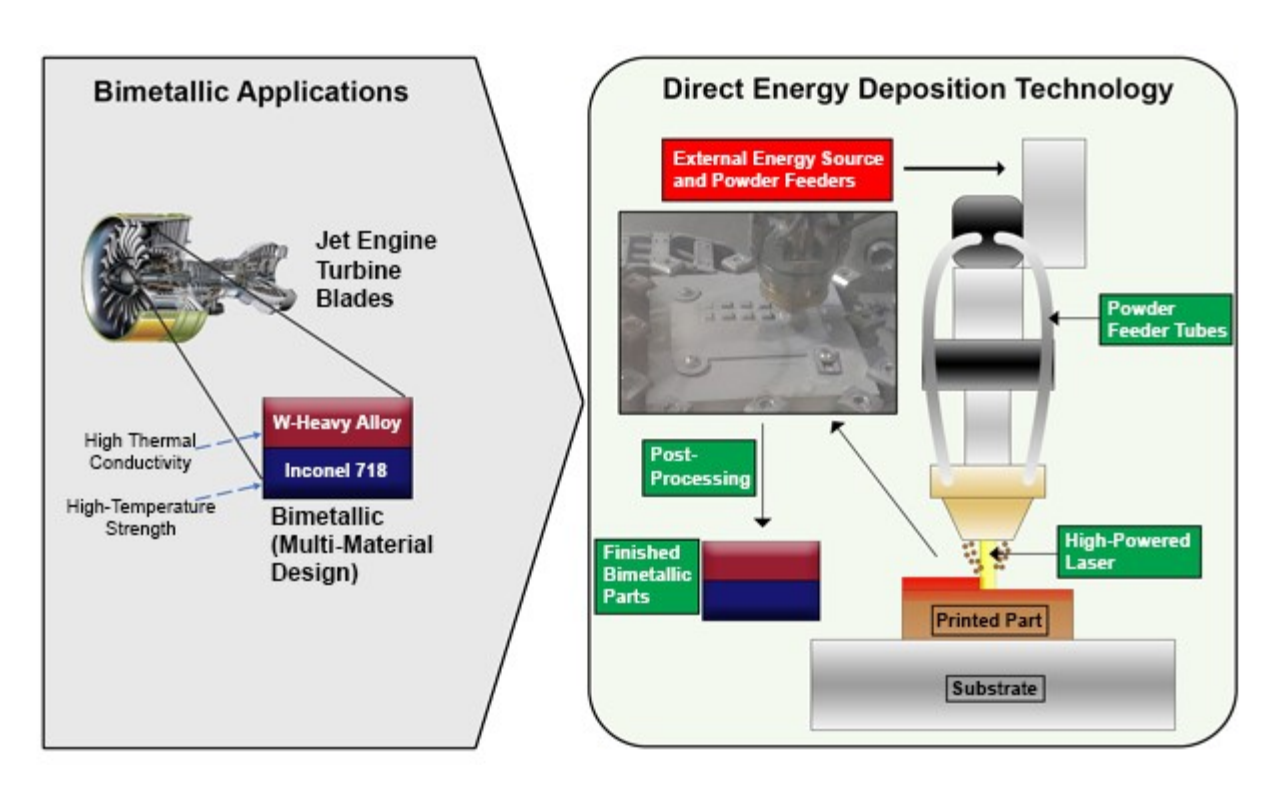


**Figure 1**: (Left) Possible application (turbines blade) of bimetallic materials. Reproduced from [21] under creative commons license. (Right) Schematic of the DED-based AM.

## 2.0 Materials and methods

2.1. Directed energy deposition (DED) of bimetallic structures: Bimetallic structures were manufactured using a FormAlloy powder-based DED AM system. The DED system takes a computer-aided design (CAD) file from the user, which outlines the part's size and shape. The DED system creates the necessary tool path to print the part. These changeable parameters include speed, layer thickness, laser power, powder flow rate, and shield gas flow rate. Furthermore, different printing substrates can be used, with common substrates being stainless steel and commercially pure titanium (CpTi). For this research, a 316L stainless steel substrate was used. Inconel 718 powder (Powder Alloy Corporation, Ohio) with a mesh size of -100/+325 was used. The tungsten alloy powder (90wt% W, 7wt% Ni, and 3wt% Ni) used was manufactured through gas atomization and spray dry processing of the alloying elements, producing a spray-dried powder having a particle size of 45 to 150 microns and spherical. Before making a batch of each bimetallic structure, various build parameters were experimented with until the final dimensions were close to the theoretical dimensions. The final parameters are

shown in Table 1. Additionally, the energy per unit volume (E) applied by the laser for each of the samples can be calculated using the following equation [22]:

$$E = \frac{P}{vht} \tag{1}$$

Where P = laser power, v = scan speed, h = layer thickness, and t = hatch distance. For example, in the thermal bimetallic sample, the energy per unit volume applied for the Inconel 718 part was  $350 \text{ J/mm}^3$  and  $562.5 \text{ J/mm}^3$  for the W7Ni3Fe part equation.

**Table 1**: Optimal and final parameters for each of the bimetallic structures. The layer thickness and hatch distance for each sample were 0.1 mm and 0.6, respectively.

Type of Sample	Inconel 718 Scanning Speed (mm/min)	W7Ni3Fe Scanning Speed (mm/min)	Inconel 718 Laser Power (W)	W7Ni3Fe Laser Power (W)	Inconel 718 Flow Rate (mm/sec)	Tungsten Flow Rate (mm/sec)
Thermal Bimetallic	1000	800	350		0.5	
W7Ni3Fe Compression	N/A	700	N/A	450	N/A	1
Sample Inconel 718	1600	N/A	350	N/A	0.5	N/A
Compression Sample						
Longitudinal Bimetallic Compression Sample	. 1200	1200	350	450	0.5	0.9
Transverse Bimetallic Compression Sample						

2.2. Characterization of bimetallic structures: First, one of the bimetallic samples was cut in half using a low-speed diamond saw. Then, the sample was ground to 1000 grit with SiC grinding paper then polished to  $0.05~\mu m$  using an alumina-DI water suspension. The sample was then imaged using a field emission scanning electron microscope (FESEM, FEI-SIRION,

Portland, OR). Element maps at the Inconel 718 – Tungsten alloy interface were also obtained using the electron dispersal spectroscopy (EDS, EDAX) SEM attachment. SEM photos of each of the sections are shown in **Figure 2**. Next, a hardness test was conducted along the interface using a Phase II Micro Vickers Hardness Tester (with 0.98N load and 15 sec dwell time). Finally, compression tests were done using an Instron compression tester (1.3 mm/min speed) for each base material and the transverse and longitudinal bimetallic samples.

A Netzsch LFA 447 Nanoflash (Germany) thermal diffusivity system was used for the thermal analysis. Four samples were tested; 2 were the base materials, with the others being two bimetallic samples. Each sample was ground to an approximate dimension of 10x10 mm with a thickness of about 2 mm. Due to the large interface size and the small thickness required for the thermal testing, most of the bimetallic sample was the interfacial region for that test. The volume percent of each material present in the bimetallic was determined through Archimedes testing.

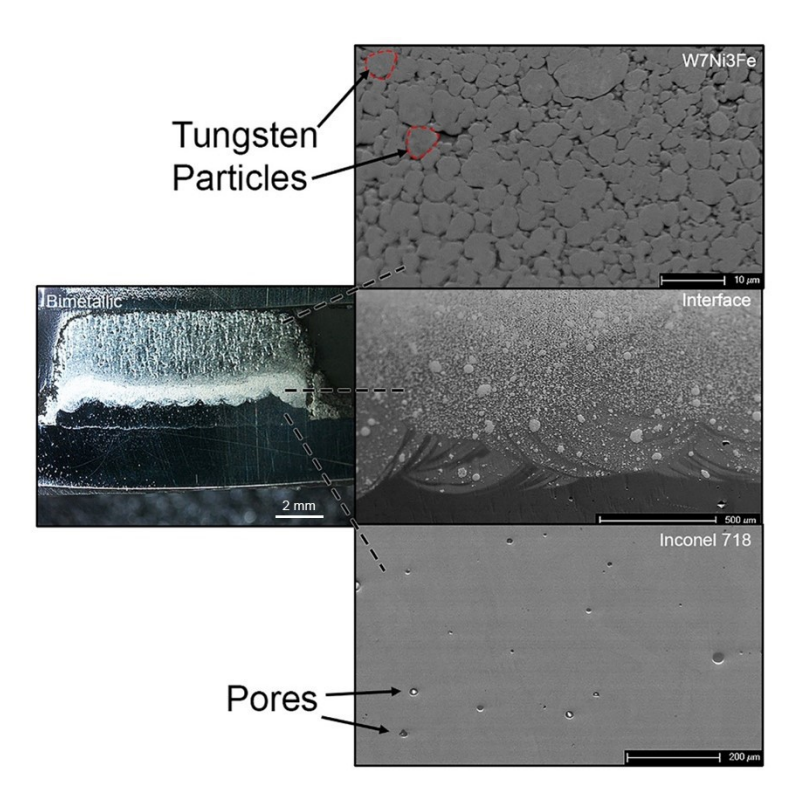


**Figure 2**: SEM Images of each of the bimetallic sections. These are taken at the magnification, which best shows the characteristics of each section. Note that the bottom part of the bimetallic that is not marked is the 316L stainless steel substrate.

#### 3.0 Results

As described above, several tests were conducted, including SEM/EDS mapping and imaging, Vickers hardness testing, compression testing, and thermal testing. The SEM/EDS mapping and imaging allowed the interface to be analyzed from a qualitative perspective, while the interfacial hardness test allowed for analysis from a quantitative perspective. The bimetallic samples used in the compression and thermal tests showed significant improvement to pure Inconel 718.

3.1. Microscopy and compositional analysis: Figure 3 shows the SEM/EDS results for the bimetallic structure. Inconel 718 adhered very well to the 316L stainless steel substrate and formed a very discrete interface. Furthermore, no cracking or irregularities were observed at the 316L interface for each material. The Inconel 718 region shows a uniform structure with very few small pores. The interface is observed to be very broad, which specifically stretches about 1.5 mm in length. Surprisingly, no porosity is observed in this section. The interface's tungsten particles' size is much smaller than the 45-150 µm particle. This is most likely due to residual stress breaking down the particles further during the printing process, combined with the partial melting, which left smaller remnants of larger particles. Also, some porosity is seen throughout the sample.

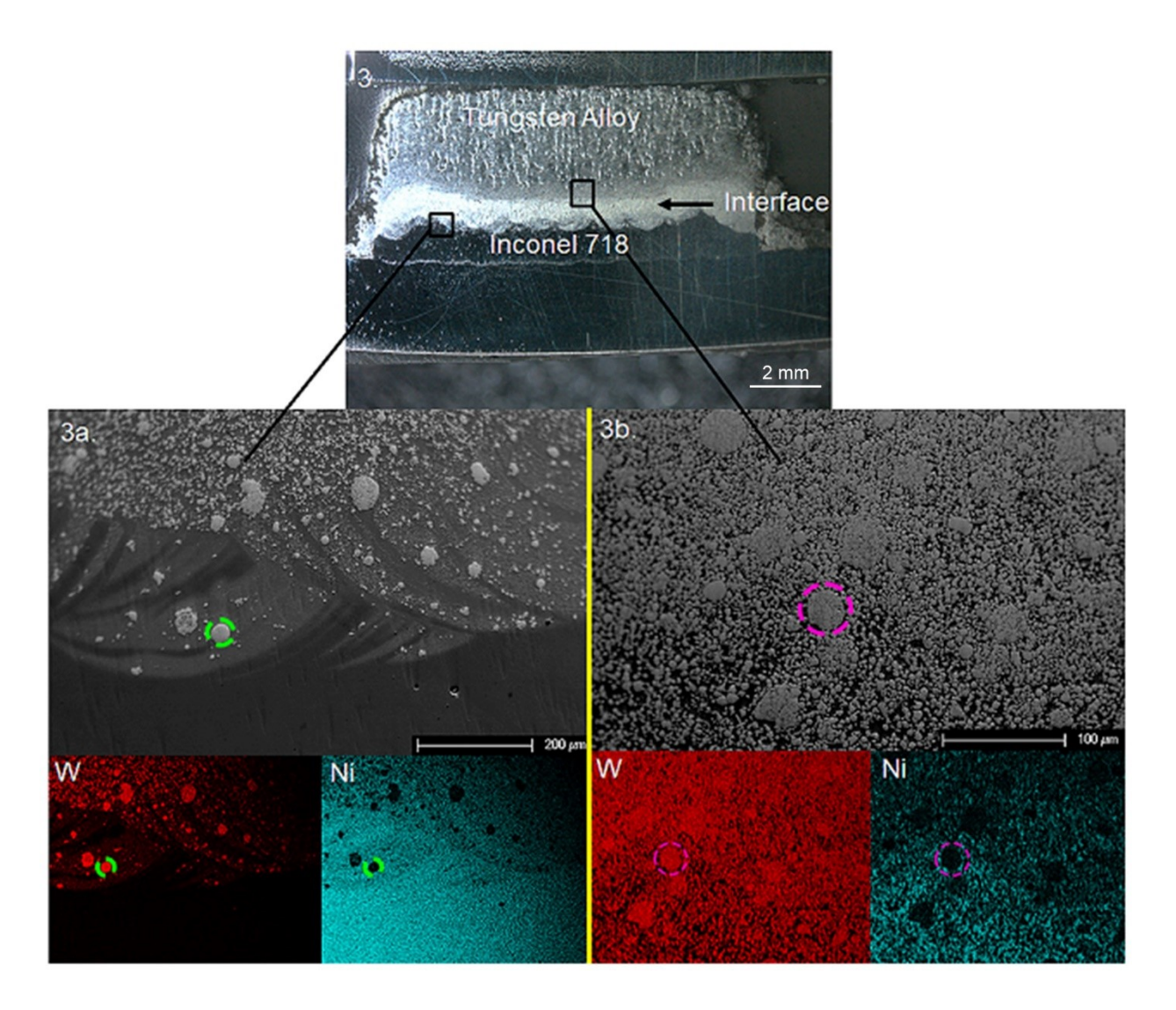
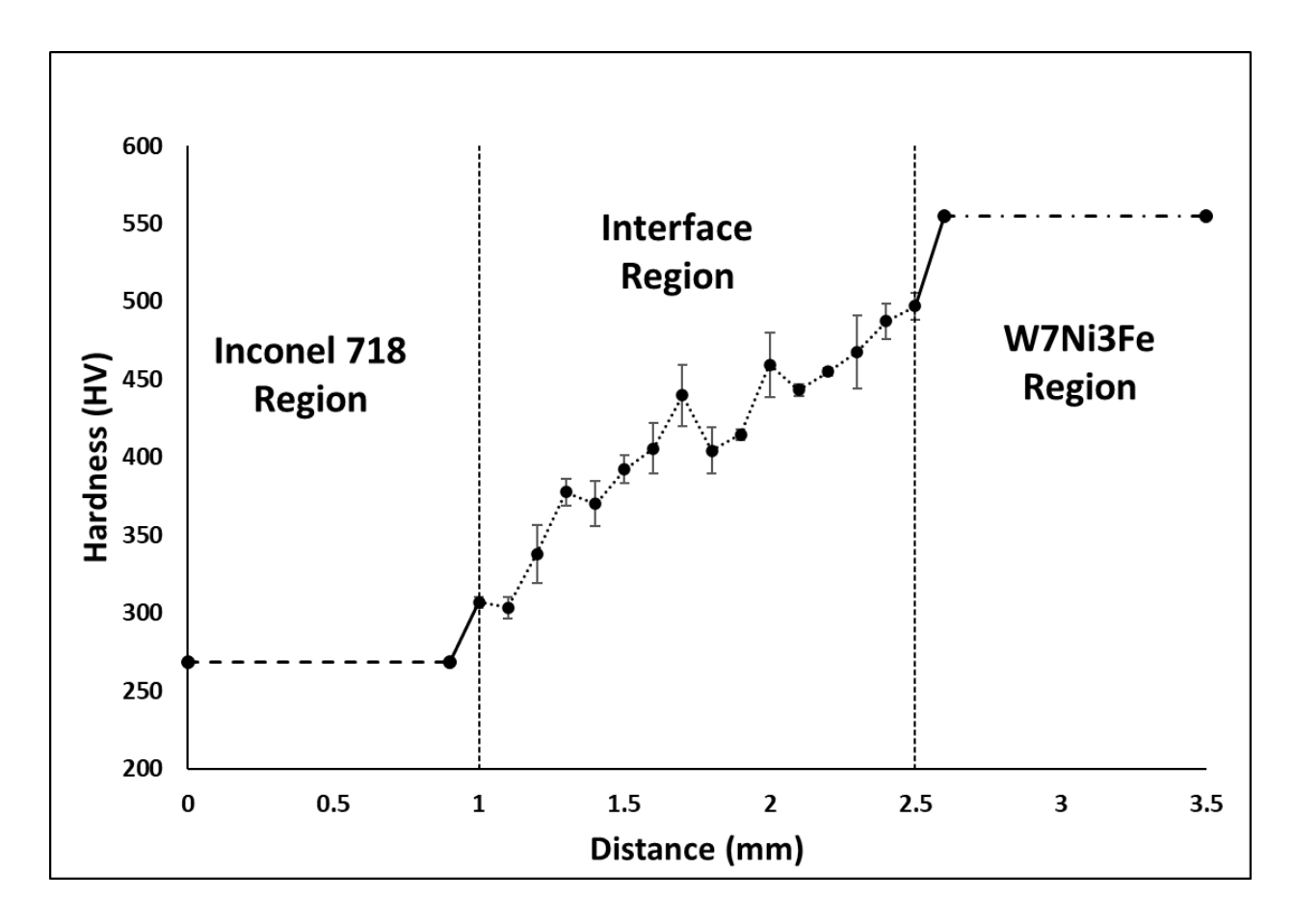


Figure 3: Stereoscope image of the cross-section of the printed bimetallic. 3a. SEM micrograph and EDS mapping of the bottom-middle part of the interface. 3b. Bottom-top part of the interface. A reference tungsten particle is circled in 3a and 3b (Green in 3a. and pink in 3b.). All nickel EDS maps are from  $K\alpha$  characteristic x-rays, while all tungsten maps are  $L\alpha$  characteristic x-rays.

3.2. *Interfacial hardness*: The hardness test results are shown in **Figure 4**. The Inconel 718 and W7Ni3Fe base samples had a hardness of 269HV and 555HV, respectively. Note that the base material region values are based on the average value of 10 hardness tests taken in just those base materials. It is observed that the interface region follows a positive linear trend, which suggests uniformity and a lack of intermetallic formation. It is common to see a spike in hardness

due to intermetallic formation [23]. This statement is backed up qualitatively from **Figure 2**, which visually shows a very uniform gradient in tungsten particles at the interface.



**Figure 4**: Hardness profile of the interface. Three different trials were done along with the interface, with a measurement being taken every 0.1 mm.

3.3 Compression tests: The compression test results of the different bimetallic and base materials are shown in **Figure 5**. These samples were tested as printed; no heat treatment was used for any sample. The primary purpose of these tests was to determine the integrity of the interface and make sure that it was not weaker than both base materials. The yield strength of the longitudinal sample was determined to be 774 MPa, with the yield strength of the transverse sample being 785 MPa, which significantly exceeds the yield strength of Inconel 718, which was 312 MPa. However, the modulus of elasticity of the bimetallic samples was about 45% lower than Inconel 718.

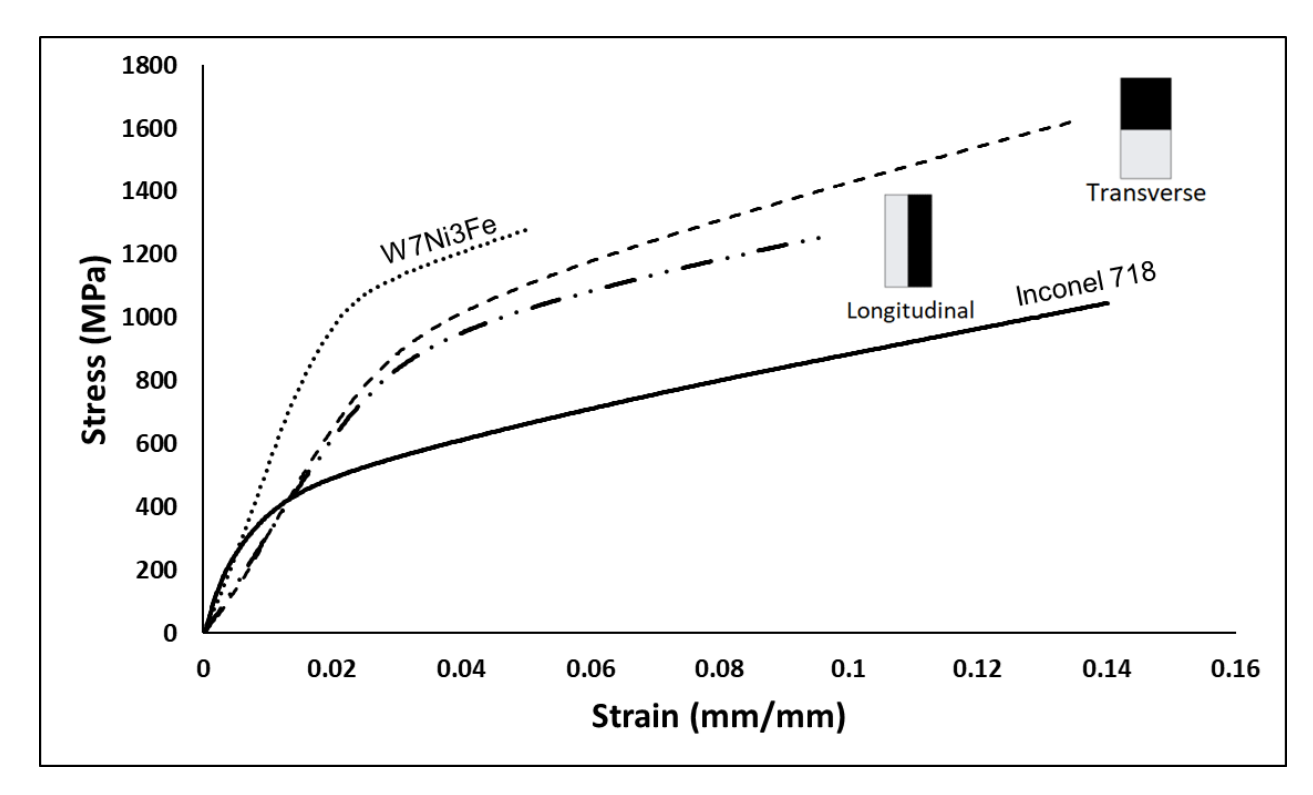


**Figure 5**: Compression Test results for the different bimetallic structures compared to each base material. Each material was tested until the force limit of the machine was reached, except for the Inconel sample, which showed no signs of breaking.

**Figure 6** shows the compressed surfaces of the transverse and longitudinal samples. The Inconel region shows the most plastic deformation in both samples as shear bands are present. Apart from a few tiny cracks, the interface region in both samples showed no signs of failure, which is the case for the tungsten alloy region as well.

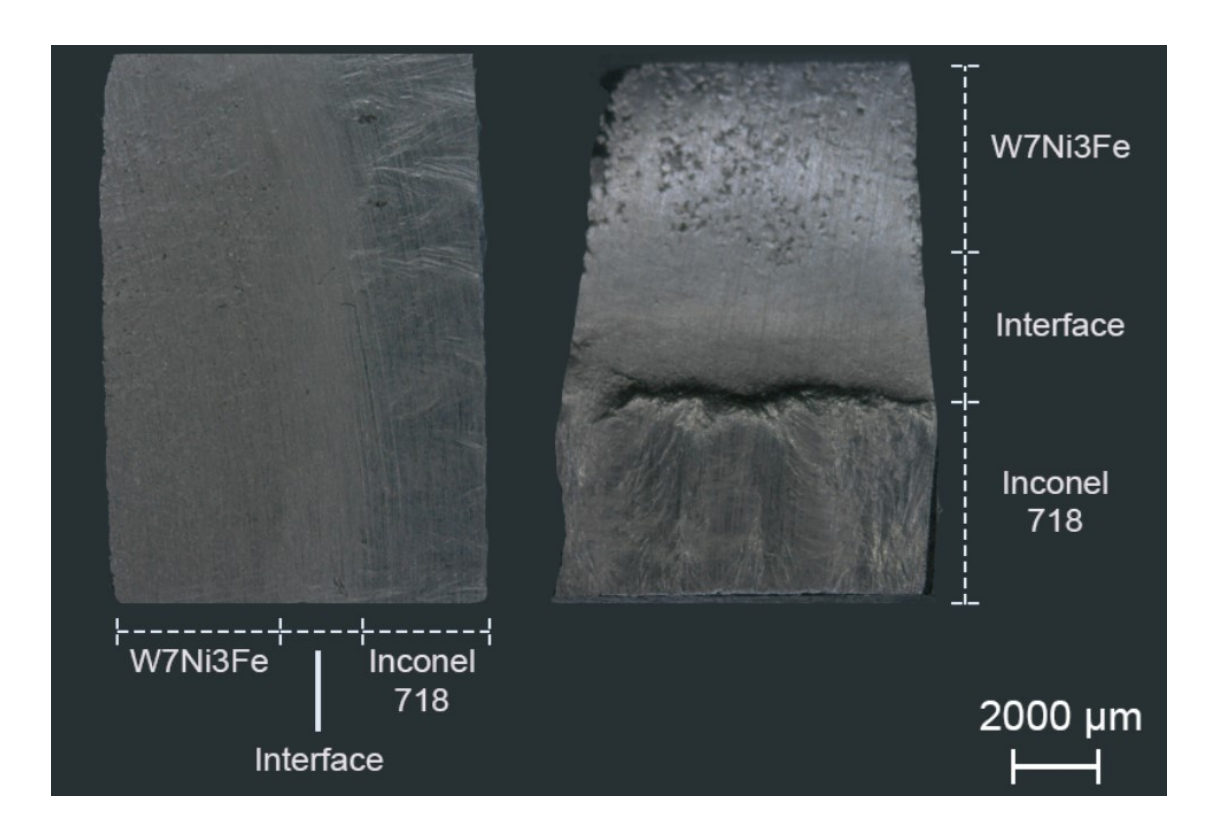


**Figure 6**: Compressed surfaces of the longitudinal sample (left) and transverse sample (right). Shear band type failure in the Inconel region is observed in both sample

<u>3.4 Thermal diffusivity</u>: The thermal diffusivity results are shown in **Figure 7**. Each of the samples showed increased thermal diffusivity with an increase in temperature. As expected, the tungsten alloy performed better than Inconel 718, with a thermal diffusivity value of 15.2-16.5 mm<sup>2</sup>/s compared to 3.00-3.8 mm<sup>2</sup>/s. The first bimetallic, composed of about 50% Inconel by volume, performed around 100% better than Inconel 718 with a value of 5.9-7.2 mm<sup>2</sup>/s. The second bimetallic, which contained 30% Inconel by volume, performed 140% better than Inconel 718 with a value of 7.8-9.1 mm<sup>2</sup>/s.

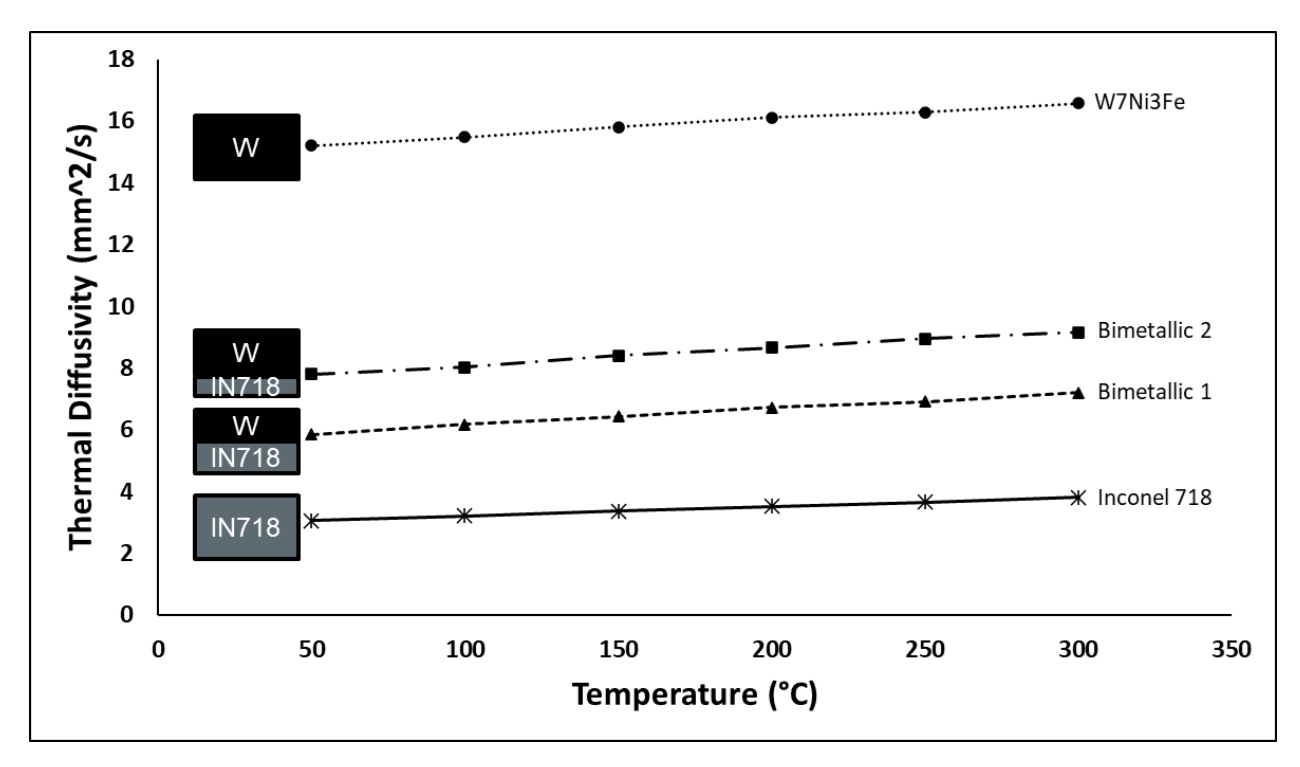


**Figure 7**: Thermal diffusivity of Inconel 718, Tungsten Alloy, and two bimetallic samples. The first sample contains about 50% Inconel 718 by volume, and the second sample contains about 30% Inconel 718 by volume.

## 4.0 Discussion

Based on our results, it is shown that DED-based AM can successfully print W7Ni3Fe onto Inconel 718 with little to no defects. The ability to print a bimetallic with a high-temperature alloy like W7Ni3Fe allows DED to stand out compared to other welding methods such as complex plasma are welding and other conventional methods. Although the bimetallic exhibited better properties than pure Inconel 718, unique characteristics are observed in each of these bimetallic structures. One such characteristic included an interface much more prominent than typical bimetallic interfaces observed in the literature [8,20], and another was the inability to print Inconel 718 onto W7Ni3Fe. Furthermore, the large gradient in the interface made it difficult to know the exact amount of each material in the test samples and made post-processing more difficult overall.

The unusual observations in these experiments were the large interface formed and the smaller size of the Inconel region, contrary to many other bimetallic studies [8, 24]. For the compression tests, this large interface appeared to enhance the strength of the bimetallic further. After parameter optimization, both Inconel and Tungsten parts alone showed no signs of underbuilding or overbuilding, meaning that the theoretical height of the parts (based on the prescribed layer thickness and the number of layers printed) is close to the same as the actual height. It is also clear that tungsten particles diffused into the Inconel 718 region, as shown in Figure 2. The most plausible explanation is that the combination of the large melt pool and the high density of the tungsten particles (~19 g/cc) caused them to sink into that region. The higher power of the Tungsten alloy part of the print likely caused an even larger melt pool to form. Also, more residual stress is created due to the material being deposited in powder form, which promotes diffusion and results in a broader interface [25]. Furthermore, micro-pools of nickel and iron in the W7Ni3Fe help with diffusion. In **Figure 7**, this process is shown in more detail. As a result, the finished structures resemble a smooth functionally graded rather than a bimetallic structure, albeit the exact compositional gradient is unknown. However, the smooth gradient in the EDS maps and the hardness test back this claim up.

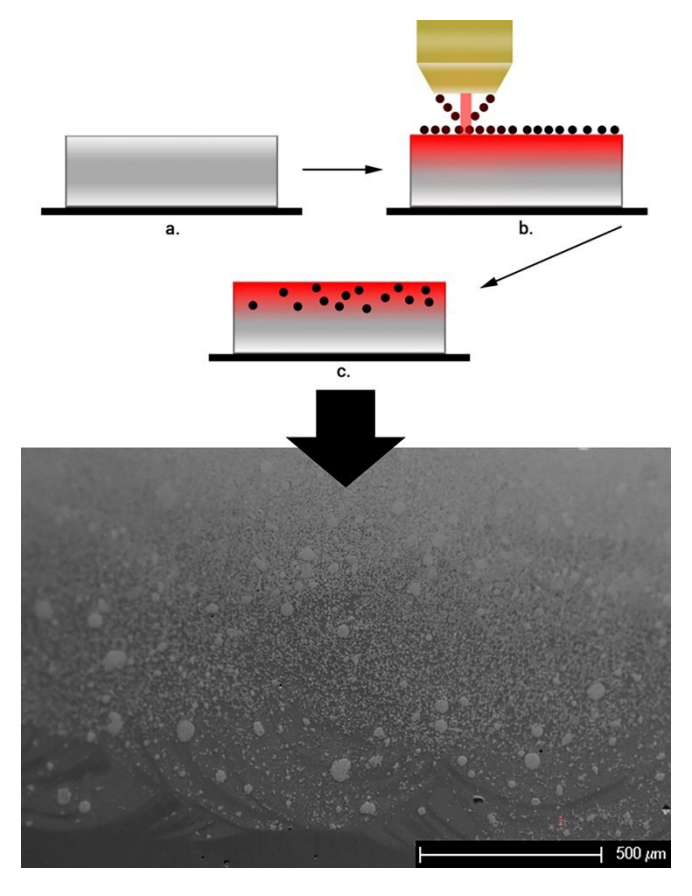


**Figure 8**: (a) Inconel 718 part of the bimetallic print. (b) The first layers of the Tungsten alloy part are printed, which causes a melt pool in both materials. (c) As a result of the high density of the tungsten particles and the melt pool, the tungsten particles sink into the Inconel part and form the interface. (Bottom) SEM micrograph of the entire printed interface. Remember that due to the high cooling rate of DED, small melt columns are created then quickly solidified, which are combined to show a melt layer in the figure for visual purposes.

Deposition of the Tungsten alloy onto Inconel 718 proved to be relatively straightforward as no cracks or irregularities were formed during the printing process, even during early optimization tests. Many other studies show cracking during part optimization [10]. However, deposition of Inconel 718 onto the W7Ni3Fe part did not work in any case and resulted in the crack formation in the middle of the tungsten alloy. This is likely due to the laser power of the Inconel 718 part being 100 W lower than the W7Ni3Fe part, which in turn was not able to initiate a sufficient melt pool for the Inconel material diffuse into the high-melting temperature of Tungsten. The melt pool was also reduced due to the high thermal conductivity of W7Ni3Fe,

which dissipated the heat quickly (the opposite would occur for Inconel 718 due to low thermal conductivity). Printing an interlayer of the two alloys mixed ended up with the same result. Therefore, the one-time parameter setup was used for each of the bimetallic. One of the cracked bimetallic is shown in **Figure 9**.

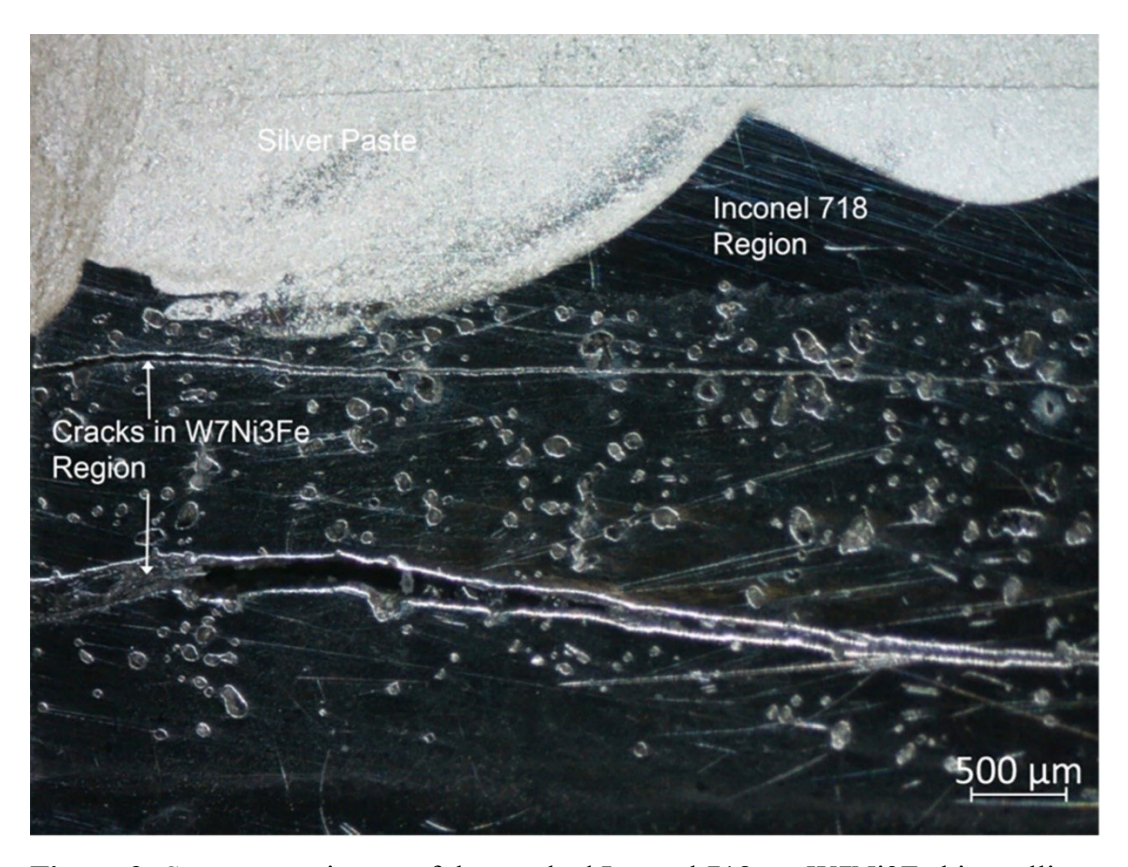


Figure 9: Stereoscope image of the cracked Inconel 718-on-W7Ni3Fe bimetallic.

Post-processing of the bimetallic structures proved to be quite a challenge. Due to the poor machinability of Inconel 718 [26] and the high strength and hardness of the Tungsten alloy, cutting via a low-speed diamond saw was inefficient. For this method, all sides would need to be ground down due to the inferior surface finish of DED printed samples. The poor surface finish made it impossible to print 2mm thick samples. Then, for a 10 mm by 10 mm sample, two cuts would need to be made to produce one bimetallic sample for thermal testing. Each cut would take upwards of an entire day to complete. Therefore, it was more efficient to manually print 6mm tall bimetallic samples and grind them down to around 2mm thickness. However, the most significant issue was to predict how much tungsten was in these samples as it consisted mainly of the interface around 1.5mm in length for each of them. As a result, there was no other way to

ensure the sample mainly consisted of the interface but to conduct an Archimedes test to determine the exact composition.

As seen in **Table 1**, the printing speed and powder feed rate varied with the different base materials and bimetallic despite the material staying the same. For the 17 mm tall Inconel sample, a large amount of overbuilding was observed during optimization despite the sample parameters as the bimetallic used for thermal testing. This is due to the poor thermal conductivity of Inconel, which caused the sample to stay hot and retain a higher percentage of the powder from the deposition head. Therefore, the optimized properties retained at the end caused the part to underbuild at first but ended at a slight overbuild to balance out, which was achieved by slightly increasing the speed. The tungsten alloy's speed needed to be reduced due to the high thermal conductivity and tall height.

As stated previously, proper literature review and building upon previous work aids in the improvement of new materials or structures. Our past work by Onuike et al. also improved upon Inconel 718's thermal diffusivity [20]. GrCop-84 (copper alloy) was used in the study instead of W7Ni3Fe as the depositional coating. GrCop-84 exhibits a higher thermal diffusivity than W7Ni3Fe, with a value of 45.67 mm²/s compared to 15.2 mm²/s at 50°C. The Inconel 718 – GrCop 84 bimettallic was found to have a thermal diffusivity of 10.3 mm²/s compared to 7.8 mm²/s for the Inconel 718 – W7Ni3Fe bimetallic. The hardness of the Inconel 718 – GrCop 84 interface displayed a non-linear trend in the interface as intermetallics were formed. As a result, the hardness peaked at ~300HV in the center of the interface in contrast to the Inconel 718 – W7Ni3Fe interface exhibiting a linear increase in hardness between 270 – 555 HV. Overall, the GrCop 84 bimetallic displayed a higher thermal conductivity/diffusivity, but the W7Ni3Fe bimetallic is mechanically stronger. Furthermore, a study on copper and Inconel 625 bimetallic showed a 100% increase in thermal diffusivity to Inconel 625, which makes it similar to the increase in thermal diffusivity found in our study [8]. In all cases, the studies displayed the benefits of the bimetallic approach when improved material performance is desired.

Compared to other studies using the same materials, significant differences and similarities in mechanical performance and microstructure were observed. First, the W7Ni3Fe microstructure was similar to other studies, even when the alloy was manufactured using other

methods such as liquid phase or spark plasma sintering, as it should be since the tungsten particles are either partially melting or not melting at all [16, 27, 28]. For the Inconel part, it was determined unnecessary to look into the microstructure in this study since many studies looked in-depth at the microstructures of Inconel 718 manufactured by DED [29, 30, 31]. In terms of mechanical properties, the hardness of W7Ni3Fe varies significantly, with some studies reporting about 250HV and some studies reporting about 500HV [32, 33] compared to the 550HV hardness of W7Ni3Fe found in this study. This is likely due to the high cooling rate of the DED-based AM process, especially for W7Ni3Fe, since this alloy can dissipate heat quickly. No other studies have looked into the hardness of W7Ni3Fe manufactured via DED. For Inconel 718, other studies have reported hardness values between 200 and 300 HV, which is similar to the 269 HV of Inconel 718 found in this study [34]. No compression data was found for both of these materials. It is important to note that no further heat treatment was done on these samples after DED processing. Heat treatments such as hot isostatic pressing can further improve these structures' mechanical properties if necessary [35].

#### 5.0 Conclusion

Various types of bimetallic structures consisting of Inconel 718 and a tungsten alloy were successfully manufactured using DED-based additive manufacturing. These samples contained no cracks or abnormalities even from the beginning of optimization when W-7Ni-3Fe was printed on Inconel 718 and contained an interface proven to be much stronger than Inconel 718 alone. It was found that the bimetallic sample consisting of around 50% Inconel 718 and 50% Tungsten alloy showed an increase in thermal diffusivity of about 100%, while the 30% Inconel 718 and the 70% Tungsten alloy showed an increase of about 140%. For the other bimetallic sample consisting of 30% Inconel 718, a 150% increase in thermal diffusivity was observed. A 150% increase in yield strength was observed for the compression samples in the bimetallic samples despite a 45% reduction in elastic modulus. Hardness data showed a linear increase in hardness throughout the interface. The SEM/EDS data showed an even increase in tungsten particle density and, combined with the hardness data, demonstrated the bimetallic structure to be similar to a typical functionally graded structure.

# **6.0 Acknowledgments**

The authors would like to acknowledge financial support from the National Science Foundation under the grant number NSF-CMMI 1934230 and the Joint Center for Aerospace Technology Innovation (JCATI, Seattle, WA) grant in collaboration with the Boeing Company (Seattle, WA). The authors would also like to acknowledge financial support from JCDREAM (Seattle, WA) towards purchasing metal additive manufacturing facilities at WSU. The authors would also like to acknowledge Tungsten Parts Wyoming, Inc., for providing the tungsten powders used in this study.

# 7.0 Data availability statement

Data will be available upon request.

#### 8.0 Conflict of interest

The authors declare no conflict of interest.

#### 9.0 References

- [1] Rajak, Dipen Kumar, Durgesh D. Pagar, Ravinder Kumar, and Catalin I. Pruncu. "Recent Progress of Reinforcement Materials: A Comprehensive Overview of Composite Materials," *Journal of Materials Research and Technology* 8, no. 6 (2019): 6354–74. <a href="https://doi.org/10.1016/j.jmrt.2019.09.068">https://doi.org/10.1016/j.jmrt.2019.09.068</a>.
- [2] Sahasrabudhe, Himanshu, Susmita Bose, and Amit Bandyopadhyay. "Laser Processed Calcium Phosphate Reinforced CoCrMo for Load-Bearing Applications: Processing and Wear Induced Damage Evaluation," *Acta Biomaterialia* 66 (2018): 118–28. https://doi.org/10.1016/j.actbio.2017.11.022.
- [3] Li, J. C., X. Lin, N. Kang, J. L. Lu, Q. Z. Wang, and W. D. Huang. "Microstructure, Tensile and Wear Properties of a Novel Graded Al Matrix Composite Prepared by Direct Energy

- Deposition," *Journal of Alloys and Compounds* 826 (2020): 154077. https://doi.org/10.1016/j.jallcom.2020.154077.
- [4] Loh, Giselle Hsiang, Eujin Pei, David Harrison, and Mario D. Monzón. "An Overview of Functionally Graded Additive Manufacturing." *Additive Manufacturing* 23 (2018): 34–44. <a href="https://doi.org/10.1016/j.addma.2018.06.023">https://doi.org/10.1016/j.addma.2018.06.023</a>.
- [5] Bobbio, Lourdes D., Richard A. Otis, John Paul Borgonia, R. Peter Dillon, Andrew A. Shapiro, Zi-Kui Liu, and Allison M. Beese. "Additive Manufacturing of a Functionally Graded Material from Ti-6Al-4V to Invar: Experimental Characterization and Thermodynamic Calculations." *Acta Materialia* 127 (2017): 133–42. https://doi.org/10.1016/j.actamat.2016.12.070.
- [6] Carroll, Beth E., Richard A. Otis, John Paul Borgonia, Jong-ook Suh, R. Peter Dillon, Andrew A. Shapiro, Douglas C. Hofmann, Zi-Kui Liu, and Allison M. Beese. "Functionally Graded Material of 304L Stainless Steel and Inconel 625 Fabricated by Directed Energy Deposition: Characterization and Thermodynamic Modeling." *Acta Materialia* 108 (2016): 46–54. https://doi.org/10.1016/j.actamat.2016.02.019.
- [7] Beyerlein, I.J., Mara, N.A., Wang, J. *et al.* Structure–Property–Functionality of Bimetal Interfaces. *JOM* **64**, 1192–1207 (2012). https://doi.org/10.1007/s11837-012-0431-0
- [8] Pan, Tan, Xinchang Zhang, Tomoya Yamazaki, Austin Sutton, Wenyuan Cui, Lan Li, and Frank Liou. "Characteristics of Inconel 625—Copper Bimetallic Structure Fabricated by Directed Energy Deposition." *International Journal of Advanced Manufacturing Technology* 109, no. 5/6 (July 21, 2020): 1261–74. https://doi.org/10.1007/s00170-020-05713-z.
- [9] Chen, Jie, Yongqiang Yang, Changhui Song, Mingkang Zhang, Shibiao Wu, and Di Wang. "Interfacial Microstructure and Mechanical Properties of 316L /CuSn10 Multi-Material Bimetallic Structure Fabricated by Selective Laser Melting." *Materials Science and Engineering:* A 752 (2019): 75–85. <a href="https://doi.org/10.1016/j.msea.2019.02.097">https://doi.org/10.1016/j.msea.2019.02.097</a>.
- [10] Onuike B. and Bandyopadhyay A., "Additive manufacturing of Inconel 718 Ti6Al4V bimetallic structures," *Additive Manufacturing*, **22**, pp. 844-851 (2018).

- [11] Shakerin, Sajad, Mehdi Sanjari, Babak Shalchi Amirkhiz, and Mohsen Mohammadi. "Interface Engineering of Additively Manufactured Maraging Steel-H13 Bimetallic Structures." *Materials Characterization* 170 (2020): 110728. <a href="https://doi.org/10.1016/j.matchar.2020.110728">https://doi.org/10.1016/j.matchar.2020.110728</a>.
- [12] Blakey-Milner, Byron, Paul Gradl, Glen Snedden, Michael Brooks, Jean Pitot, Elena Lopez, Martin Leary, Filippo Berto, and Anton du Plessis. "Metal Additive Manufacturing in Aerospace: A Review." *Materials & Design* 209 (2021): 110008. https://doi.org/10.1016/j.matdes.2021.110008.
- [13] Shang, Chun, Chenyang Wang, Guojian Xu, Changfu Li, and Junhua You. "Laser Additive Manufacturing of TA15 Inconel 718 Bimetallic Structure via Nb/Cu Multi-Interlayer." *Vacuum* 169 (2019): 108888. <a href="https://doi.org/10.1016/j.vacuum.2019.108888">https://doi.org/10.1016/j.vacuum.2019.108888</a>.
- [14] Li, Guangyu, Wenming Jiang, Feng Guan, Junwen Zhu, Zheng Zhang, and Zitian Fan. "Microstructure, Mechanical Properties and Corrosion Resistance of A356 Aluminum/AZ91D Magnesium Bimetal Prepared by a Compound Casting Combined with a Novel Ni-Cu Composite Interlayer." *Journal of Materials Processing Technology* 288 (2021): 116874. https://doi.org/10.1016/j.jmatprotec.2020.116874.
- [15] Y. Şahin, "Recent Progress in Processing of Tungsten Heavy Alloys", *Journal of Powder Technology*, vol. 2014, Article ID 764306, 22 pages, 2014. https://doi.org/10.1155/2014/764306
- [16] C. Henager et al., "Recent Progress in the Development of Ductile-Phase Toughened Tungsten for Plasma-Facing Materials: W-Ni-Fe Composites," June 2015, DOI: <a href="https://web.archivec.nlm.nual-progress">10.13140/RG.2.1.2088.4960</a>, In book: Fusion Reactor Materials Program Semiannual Progress Reports DOE/ER-0313/58, Chapter: 4.2, Volume 58, <a href="http://web.ornl.gov/sci/physical\_sciences\_directorate/mst/fusionreactor/Vol58.shtml">http://web.ornl.gov/sci/physical\_sciences\_directorate/mst/fusionreactor/Vol58.shtml</a>].
- [17] Hall, Loura. "Conventional and Flash Sintering of Tungsten and Tungsten Alloys." Text. NASA, January 7, 2021. <a href="http://www.nasa.gov/directorates/spacetech/strg/early-stage-innovations-">http://www.nasa.gov/directorates/spacetech/strg/early-stage-innovations-</a>

esi/esi2020/Conventional and Flash Sintering of Tungsten and Tungsten Alloys.

- [18] Schuster, Brian, Magness, Lee, and U.S. Army Research Laboratory, issuing body. *A Comparison of the Deformation, Flow, and Failure of Two Tungsten Heavy Alloys in Ballistic Impacts*. Aberdeen Proving Ground, MD: Army Research Laboratory, 2005.
- [19] Hosseini, E., and V. A. Popovich. "A Review of Mechanical Properties of Additively Manufactured Inconel 718." *Additive Manufacturing* 30 (2019): 100877. https://doi.org/10.1016/j.addma.2019.100877.
- [20] Onuike, Bonny, Bryan Heer, and Amit Bandyopadhyay. "Additive Manufacturing of Inconel 718—Copper Alloy Bimetallic Structure Using Laser Engineered Net Shaping (LENS<sup>TM</sup>)." *Additive Manufacturing* 21 (2018): 133–40. https://doi.org/10.1016/j.addma.2018.02.007.
- [21] Han, Pinlian. "Additive Design and Manufacturing of Jet Engine Parts." *Engineering* 3, no. 5 (2017): 648–52. <a href="https://doi.org/10.1016/J.ENG.2017.05.017">https://doi.org/10.1016/J.ENG.2017.05.017</a>.
- [22] Guan, Tingting, Suiyuan Chen, Xueting Chen, Jing Liang, Changsheng Liu, and Mei Wang. "Effect of Laser Incident Energy on Microstructures and Mechanical Properties of 12CrNi2Y Alloy Steel by Direct Laser Deposition." *Journal of Materials Science & Technology* 35, no. 2 (2019): 395–402. <a href="https://doi.org/10.1016/j.jmst.2018.10.024">https://doi.org/10.1016/j.jmst.2018.10.024</a>.
- [23] Yanning Zhang and Amit Bandyopadhyay, "Tailoring compositionally graded interface of 316L stainless steel to Al12Si aluminum alloy bimetallic structures via Additive Manufacturing," *ACS Applied Materials & Interfaces*, **13** (7), pp. 9174–9185 (2021). DOI?
- [24] Zakipour, Shahrokh, Ayoub Halvaee, Ahmad Ali Amadeh, Majid Samavatian, and Alireza Khodabandeh. "An Investigation on Microstructure Evolution and Mechanical Properties during Transient Liquid Phase Bonding of Stainless Steel 316L to Ti–6Al–4V." *Journal of Alloys and Compounds* 626 (2015): 269–76. <a href="https://doi.org/10.1016/j.jallcom.2014.11.160">https://doi.org/10.1016/j.jallcom.2014.11.160</a>.
- [25]: Anderson, Ryan, Terrell, Jordan, Schneider, Judy, Thompson, Sean, and Gradl, Paul. "Characteristics of Bi-Metallic Interfaces Formed During Direct Energy Deposition Additive Manufacturing Processing." Metallurgical and Materials Transactions. B, Process Metallurgy and Materials Processing Science 50, no. 4 (2019): 1921–30. <a href="https://doi.org/10.1007/s11663-019-01612-1">https://doi.org/10.1007/s11663-019-01612-1</a>.

- [26] Montazeri, Saharnaz, Aramesh, Maryam, Arif, Abul Fazal M, and Veldhuis, Stephen C. "Tribological Behavior of Differently Deposited Al-Si Layer in the Improvement of Inconel 718 Machinability." *International Journal of Advanced Manufacturing Technology* 105, no. 1 (2019): 1245–58. <a href="https://doi.org/10.1007/s00170-019-04281-1">https://doi.org/10.1007/s00170-019-04281-1</a>.
- [27] Li, Chun, Yingpei Wang, Shiyu Ma, Xiaoshan Yang, Jinfeng Li, Yuzhao Zhou, Xue Liu, Jingang Tang, Xiaoying Wang, and Guomin Le. "Densification, Microstructural Evolutions of 90W-7Ni-3Fe Tungsten Heavy Alloys during Laser Melting Deposition Process." *International Journal of Refractory Metals and Hard Materials* 91 (2020): 105254. https://doi.org/10.1016/j.ijrmhm.2020.105254.
- [28] Xiang, D. P., L. Ding, Y. Y. Li, J. B. Li, X. Q. Li, and C. Li. "Microstructure and Mechanical Properties of Fine-Grained W–7Ni–3Fe Heavy Alloy by Spark Plasma Sintering." *Materials Science and Engineering: A* 551 (2012): 95–99. <a href="https://doi.org/10.1016/j.msea.2012.04.099">https://doi.org/10.1016/j.msea.2012.04.099</a>.
- [29] Kumar, S. Pratheesh, S. Elangovan, R. Mohanraj, and J. R. Ramakrishna. "A Review on Properties of Inconel 625 and Inconel 718 Fabricated Using Direct Energy Deposition." *Materials Today: Proceedings* 46 (2021): 7892–7906. https://doi.org/10.1016/j.matpr.2021.02.566.
- [30] Yu, Xiaobin, Xin Lin, Fencheng Liu, Lilin Wang, Yao Tang, Jiacong Li, Shuya Zhang, and Weidong Huang. "Influence of Post-Heat-Treatment on the Microstructure and Fracture Toughness Properties of Inconel 718 Fabricated with Laser Directed Energy Deposition Additive Manufacturing." *Materials Science and Engineering: A* 798 (2020): 140092. https://doi.org/10.1016/j.msea.2020.140092.
- [31] Sreekanth, Suhas, Ehsan Ghassemali, Kjell Hurtig, Shrikant Joshi, and Joel Andersson. "Effect of Direct Energy Deposition Process Parameters on Single-Track Deposits of Alloy 718." *Metals* 10, no. 1 (2020). <a href="https://doi.org/10.3390/met10010096">https://doi.org/10.3390/met10010096</a>.
- [32] Gong, X., J. L. Fan, F. Ding, M. Song, and B. Y. Huang. "Effect of Tungsten Content on Microstructure and Quasi-Static Tensile Fracture Characteristics of Rapidly Hot-Extruded W–Ni–Fe Alloys." *International Journal of Refractory Metals and Hard Materials* 30, no. 1 (2012): 71–77. <a href="https://doi.org/10.1016/j.ijrmhm.2011.06.014">https://doi.org/10.1016/j.ijrmhm.2011.06.014</a>.

- [33] Xiang, D. P., L. Ding, Y. Y. Li, G. B. Chen, and Y. W. Zhao. "Preparation of Fine-Grained Tungsten Heavy Alloys by Spark Plasma Sintered W–7Ni–3Fe Composite Powders with Different Ball Milling Time." *Journal of Alloys and Compounds* 562 (2013): 19–24. https://doi.org/10.1016/j.jallcom.2013.02.014.
- [34] Chen, Bo, and Jyoti Mazumder. "Role of Process Parameters during Additive Manufacturing by Direct Metal Deposition of Inconel 718." *Rapid Prototyping Journal* 23, no. 5 (2017): 919–29.
- [35] S. Sun, Q.Teng, Y. Xie, T. Liu, R. Ma, J. Bai, C. Cai, Q.Wei, "Two-step heat treatment for laser powder bed fusion of a nickel-based superalloy with simultaneously enhanced tensile strength and ductility," Additive Manufacturing, 46, 102168 (2021). <a href="https://doi.org/10.1016/j.addma.2021.102168">doi.org/10.1016/j.addma.2021.102168</a>